Compressive strain-dependent bending strength property of Al_2O_3–ZrO_2 (1.5 mol% Y_2O_3) composites performance by HIP

A. Reyes-Rojas, H. Esparza-Ponce, S.D. De la Torre, E. Torres-Moye

Abstract

Nanometric powders and sintered ceramics of Al_2O_3–ZrO_2 (1.5 mol% Y_2O_3) prepared by hot isostatic pressing HIP have been studied. A detailed crystallographic study has been performed throughX-ray diffraction, Williamson–Hall method, Rietveld method and high-resolution electron microscopy HREM analysis.

The crystallographic structure data, such as domain size, lattice parameters, wt% phase, and microstrain direction have been obtained using Rietveld refinement and Williamson–Hall methods. The results revealed that the compressive strain (ε) increased from0.56 to 1.18 (10^{-3}) as the t-ZrO_2 content increased too.

The HREM interface study conducted along the [0 0 0 1]Al_2O_3||[0 0 1]ZrO_2 zone axis revealed a micro-strain lattice distortion accumulated at the grain boundary due to the ZrO_2 martensitic phase transformation on cooling, t-ZrO_2 grains coalescence and to the grain growth of α-Al_2O_3 which cause elongated tetragonal crystals. Micro-strain lattice distortion is adjusted by the shear displacements of the planes (1 1 0) and (1 $\bar{1}$ 0) along [$\bar{1}$ 1 0] and [$\bar{1}$ $\bar{1}$ 0] crystallographic directions, respectively; these planes are arrested by the (1 0 $\bar{1}$ 0) alumina plane. In this case, semi-coherent interfaceswere observed along the grain boundary. It is verified that the bending strength increased in connection with the strain accumulation and amount of tetragonal structure.

Keywords: ZrO_2-Al_2O_3 ceramics, Williamson-Hall, TEM, Rietveld analysis, Micro-strain.

Introduction

Zirconia-toughened alumina (ZTA) ceramics have been studied by other authors because it is high hardness, strength, toughness and chemical stability due to it is perfect in vivo chemical behavior [1–3]. This Al_2O_3/ZrO_2 ceramic is useful as insulator, refractory, cutting tools, high temperature filtering, biomedical application, etc. [4].

Undoped zirconia exhibits phase transitions from room temperature to high temperature. At room temperature the phase is monoclinic (m) and is stable up to 1205 ◦C. The tetragonal phase (t) exists between 1205 ◦C and 2377 ◦C, it is stabilized by doping with suitable cations, e.g. Y^{3+}, Sm^{3+}, Mg^{2+}, Ce^{4+}, and Ca^{2+}, which randomly occupy the cation sites of Zr, while charge balance is achieved by an appropriate number of vacancies at the O sites [5]. However, when it is mixed with alumina the solubility of Zr^{4+} in Al_2O_3 bulk is very low, and then the Zr atoms can exist only at the very narrow region of the grain boundary [6]. This phenomenon can change the inter-phase boundarymatching. Therefore, the inter-phase boundary has been analyzed by transmission electron microscopy (TEM) and HREM in order to provide more information about the structural defects closed to inter-phase boundary of the Al_2O_3–ZrO_2 (1.5 mol% Y_2O_3) composites.

The stress-induced transformation-toughening mechanism producedby the partial-stabilizedzirconia ZrO_2 is verywell known; and it originates microcracks by the transformation of particles from tetragonal to monoclinic phase [7]. The toughness of Al_2O_3–ZrO_2 composites is improved by stress-induced phase transformation and microcracks toughening of dispersed zirconia. The strength and fracture toughness

depend mainly ofAl_2O_3/ZrO_2 ratio the size of ZrO_2 grains, micro-strain and relative t-ZrO_2/m-ZrO_2 content. However, the stress has a direct relation with the strain [8].

During recent years, have appeared some contributions in the literature reporting results of the strain in Al_2O_3/ZrO_2 ceramics [9–11]. However, the amount of mol% Y_2O_3 is higher; therefore the study of Al_2O_3–ZrO_2 composites with 1.5mol% Y_2O_3 is very interesting. In addition, the strain is responsible of large variety of phenomena like toughness enhancement, slow crack growth and environmental-assisted aging. However, strain results are obtained principally by X-ray diffraction techniques; therefore, the preferred orientation phenomenon in tetragonal t-ZrO_2 crystals is possible due to their ferroelastic domain orientation [12]. Other structural defects are present such as instrumental broadening, dislocations, anti-phase domains, micro-strains and small crystal sizes, which manifest in the X-ray diffraction pattern by a broadening of the Bragg peaks. Therefore, to avoid instrumental line-broadening in this work we used a resolution function for the diffractometer.

In order to elucidate the relation between bending strength, domain size, phase content, lattice parameter change and strain on Al_2O_3–ZrO_2 (1.5 mol% Y_2O_3) composites a detailed structural analysis has been attempted using X-ray diffraction, Williamson–Hall method and Rietveld method. In this work we also examine the influence of strain orientation (tension or compression) on mechanical behavior.

Materials and methods

Nanometric powders and sintered ceramics Al_2O_3–ZrO_2 (1.5 mol% Y_2O_3) with 95–5 wt% and 87–13wt% concentrations which have reached bending strength values ranging from 700MPa to 1GPa were prepared by TRI-Osaka and details of processing

have been reported elsewhere [13]. Bending strength increased from 700MPa (normal bending) to 1GPa. In order to elucidate this increase, the powder samples with 95% (SA), 87% (SB) of Al_2O_3 and the ceramics sintering at 1575 ◦C and 1600 ◦C were chosen for this study. A detailed crystallographic study has been performed.

Average of domain size and micro-strain by XRD: The crystal structure of the sintering samples was studied by XRD in order to understand the increase of bending strength. Domain size and micro-strain were evaluated through Williamson–Hall and Rietveld methods.

It is known that in the powder XRD patterns, reflection broadening (FWHM) is attributed to the contributions of domain size, micro-strain and instrumental broadening [14]. Crystal size t is inversely proportional to the broadening (FWHM) of reflections according to the Debye–Scherrer equation [15]. In our case, the contribution to instrumental broadening was predetermined from the XRD pattern of Al_2O_3 and subtracted from the total peak width.

Combining size and micro-strain ε [16], the two broadening effects can be obtained: as size and strain using the simple straight line equation or Williamson–Hall approach:

$$\mathrm{FWHM} = \beta = \beta_t + \beta_\varepsilon = \frac{0.9\lambda}{t\cos\theta} + 2\varepsilon\left(\frac{2\sin\theta}{\cos\theta}\right)$$

$$\frac{\beta\cos\theta}{\lambda} = \frac{0.9}{t} + 2\varepsilon\left(\frac{2\sin\theta}{\lambda}\right) \quad (1)$$

where β represents full-width at half-maximum (FWHM) of XRD peaks; λ, wavelength of the X-ray; t, crystal size; ε, internal micro-strain and θ, Bragg angle.

Therefore, if β cos θ/λ is plotted versus 2 sin θ/λ from Eq. (1), the micro-strain is obtained from the slope of the line that passes through the points and particle size is determined from the ordinate intercept [17].

Domain size and micro-strain of the tetragonal phase was calculated from the study of XRD patterns, trough strongest peaks (1 0 1), (0 0 2), (1 1 2), (1 0 3), (2 0 2) and (0 0 4).

Rietveld analysis: Each sample was placed in the X-ray powder diffractometer, model X'Pert MPD (Phillips), equippedwith Cu K□monochromatic radiation, and θ–2θ geometry, using a 2θ angle range from 20◦ to 110◦ in step-scanning mode with a step length of 0.01◦ and using a step-counting time of 10 s. Structure parameters were obtained by the Rietveld method with the FULLPROF program [18], and a peak shape modified Thompson–Cox–Hasting pseudo-Voigt function for the calculated reflection profile. Reproducibility for (a) background parameters, (b) scale factors, (c) instrumental effects (zero point and sample off-centering), (d) structural parameters, (e) profile parameters, (f) domain size parameters, (g) micro-strain parameters and (h) phase quantification was considered for refinement until the results converged intominimum values. Instrumental broadenings U, V, andWwere determined from the Rietveld refinement of an X-ray diffraction pattern of the Al_2O_3 powder sample (a standard for quantitative analysis in XRD) [19]. The results were used in the refinement of all patterns by the incorporation of a new input file containing instrumental resolution function (IRF). Calculated values were U= 0.009647, V =−0.007718, andW= 0.010112. The Rietveld method was used to determine unitcell parameters and quantity of phase. The determination of domain size (or crystal size) and micro-strainswas done

considering the broadening of the Bragg reflection profile. All data for crystallographic analysis were obtained from well-known Refs. [20–24].

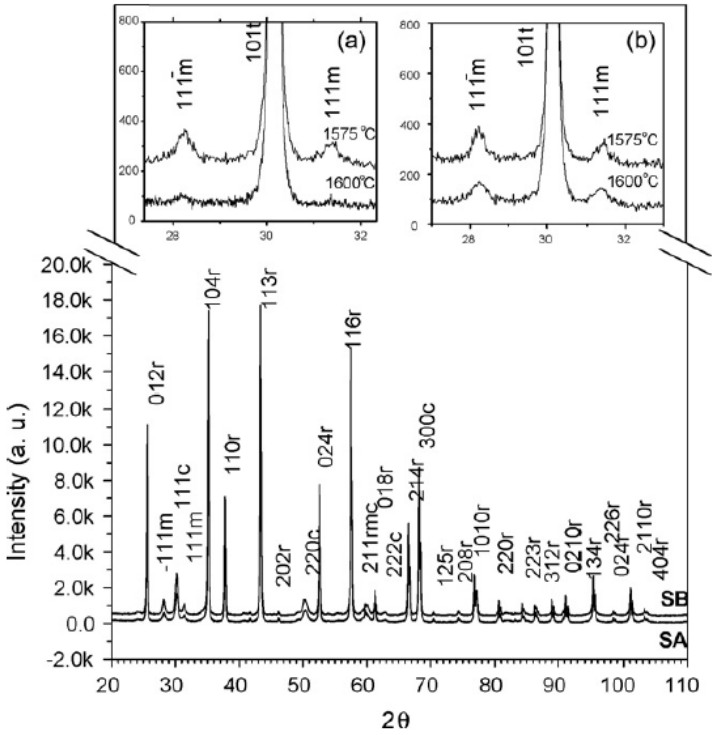

Fig. 1. X-ray diffraction patterns for Al_2O_3–ZrO_2 (1.5 mol% Y_2O_3) powders as the starting materials, where SA represents the sample with 95% of Al_2O_3 and SB 87% of Al_2O_3. Inserts (a) and (b) confirm the residue of m-ZrO_2 phase after HIP sintering for samples SA and SB, respectively.

Microstructures by TEM and HREM: Microstructures were analyzed by transmission electron microscopy. Samples were prepared by using standard techniques of mechanical grinding, dimpling and ion milling. As-received samples were prepared to obtain disc specimens of 3mm diameter and dimpled on one side with a Gatan dimpler until the central region was about 5μm thick. Final thinning to perforation was carried out with a Gatan ion-milling machine for their microstructural examination using a Jeol 4000EX operated at 400 kV with a point resolution of ≈1.7Å. The

microscope was operated carefully to ensure that grain boundary was parallel to electron beam during HREM.

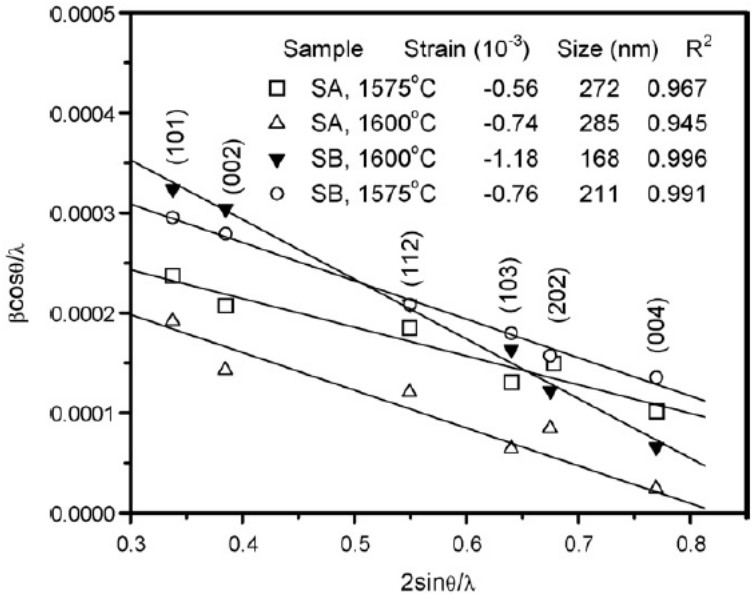

Fig. 2. Williamson–Hall plots for tetragonal crystals of the ZrO_2 (1.5 mol% Y_2O_3) solid solution. The straight lines are results of linear fit of data.

Results and discussion

Determination of domain size and micro-strain by XRD: Fig. 1 shows X-ray diffraction patterns of Al_2O_3–ZrO_2 (1.5 mol% Y_2O_3) with 95% (SA) and 87% (SB) of Al_2O_3. It clearly confirms the formation of Al_2O_3 rhombohedral phase and the ZrO_2–1.5 mol% Y_2O_3 solid solution which is principally made of cubic and monoclinic structure. The insert of Fig. 1(a) shows the sample series (SA) HIP sintering at 1575 ◦C and 1600 ◦C; in this case, cubic structure changed to tetragonal structure during the sintering process. This transformation was confirmed as other authors [25,26] by the XRD study in the region between 72◦ and 76◦ (2θ), where planes (0 0 4)t and (2 2 0)t confirmed the presence of tetragonal zirconia polycrystals (Y-PSZ) and the absence of $(4\ 0\ 0)_c$ plane confirmed the total transformation from cubic to tetragonal structure. However, there are

very small amounts of monoclinic phase at 1600 ◦C, which is formed through diffusion-less transformation from the high temperature tetragonal phase during cooling [27]. The other insert on the right side of Fig. 1(b) shows sample series (SB) sintering at same temperatures; there is similar behavior as in the samples of series (SA), however, when the amount of ZrO_2–5 mol% Y_2O_3 solid solution increases, the residual monoclinic phase increases too.

Addition of the ZrO_2–5 mol%Y_2O_3 solid solution intoAl_2O_3 polycrystals affects grain growth [28] and increases micro-strain in the tetragonal structure.

Williamson–Hall(WH)measurements showed the separation of individual contributions of size and strain for sample series SA and SB. Fig. 2 shows WH plots where $\beta \cos \theta/\lambda$ is plotted against $2 \sin \theta/\lambda$ for ceramics with 95% (SA) and 87%(SB) of Al_2O_3 sintering at 1575 ◦C and 1600 ◦C. For all cases, $\beta \cos \theta/\lambda$ shows a linear $2 \sin \theta/\lambda$ dependence and negative slopes, which indicate the presence of effective compressive micro-strain in tetragonal crystal lattices [29]. This can be caused by alumina crystals growth, which is inhibited during HIP sintering process by tetragonal crystals of the ZrO_2–1.5 mol% Y_2O_3 solid solution [30].

The study of crystallographic behavior of the (1 0 1), (0 0 2), (1 1 2), (1 0 3), (2 0 2) and (0 0 4) planes in the Williamson–Hall plots indicated that domain shape is anisotropic, so the lines are connected by two orders of plane families. The (1 0 1) and (2 0 2) crystallographic planes show a considerable slope, which indicate strong lattice distortion in the {101} plane family along [1 1 0] crystallographic direction. A similar behavior was obtained for (0 0 2) and (0 0 4) crystallographic planes indicating strong lattice distortion in the {001} plane family along [0 0 1] crystallographic direction.

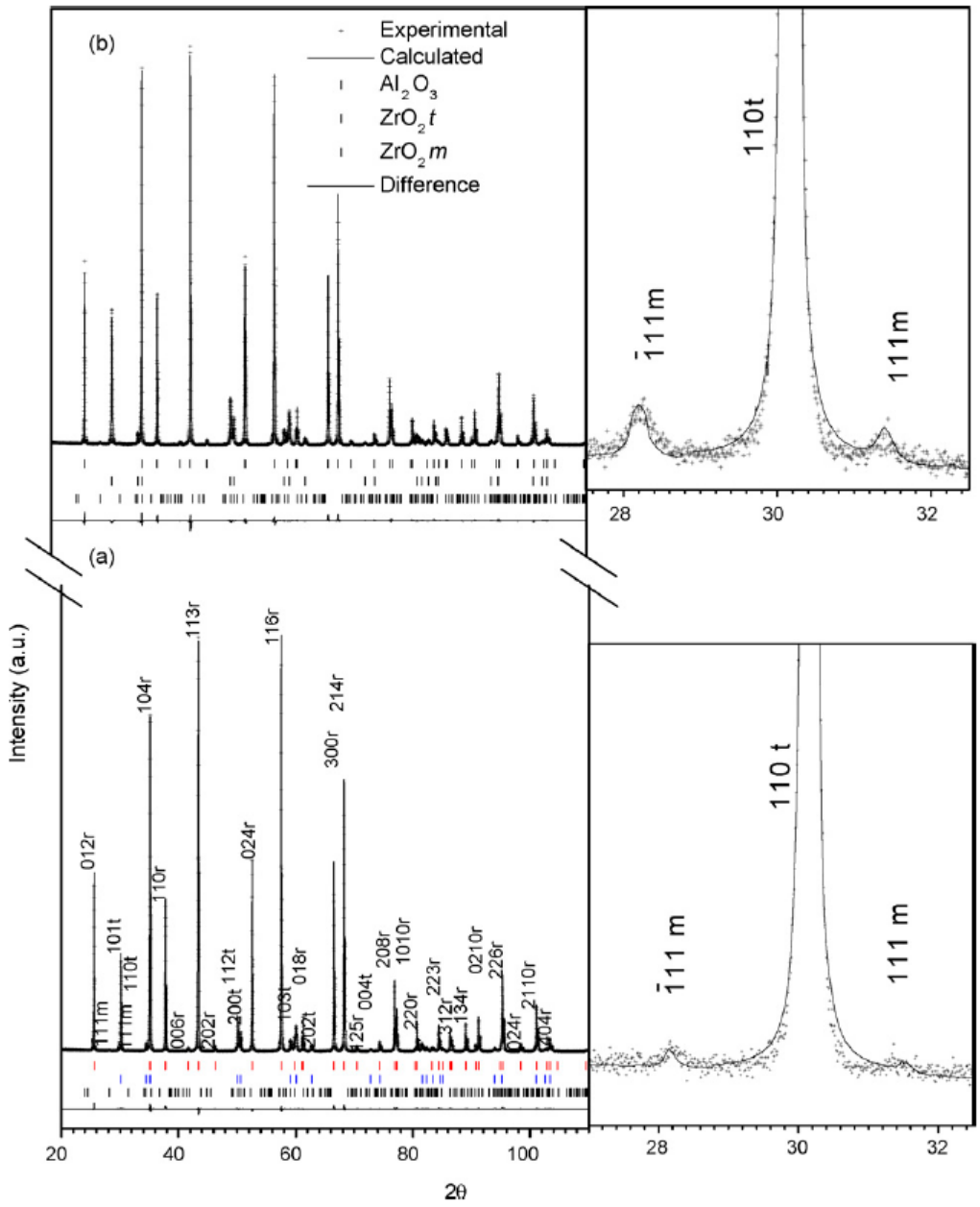

Fig. 3. Example of the experimental and calculated XRD pattern by the Rietveld method for Al_2O_3–ZrO_2 (1.5 mol% Y_2O_3) ceramics HIP sintered at 1600 °C, where (a) 95% Al_2O_3 and (b) 87% Al_2O_3. It shows an amplification of the region between 28° and 32°. Planes $(\bar{1}\,1\,1)_m$ and $(1\,1\,1)_m$ confirm the presence of the monoclinic phase.

Domain size (t) and micro-strain (ε) values obtained from intercept and WH slope plots are shownin Fig. 2 insert. It is observed that t does not change considerably, however, ε increased from−0.56 to −1.18 (10^{-3}) by a considerable amount of tetragonal crystals in the ZrO_2–1.5 mol% Y_2O_3 solid solution. This could be due, first to a slight

tetragonal distortion [31] and, second, to the difference in the elastic module that exists between the plane family {001} and {101} of tetragonal crystals.

Rietveld, size and micro-strain analysis: Results with the Rietveld method for the Al_2O_3–ZrO_2 (1.5 mol% Y_2O_3) sample series SA and SBwere obtained using the space group $Fm\bar{3}m$ for the cubic phase, $P4_2/nmc$ for the tetragonal phase, $P2_1/c$ for monoclinic phase and $R\bar{3}c$ for hexagonal phase [32]. As anexample, Fig. 3 shows the final ceramics fitting with 5% ZrO_2 (1.5 mol%Y_2O_3) (a) and 13% ZrO_2 (1.5 mol% Y_2O_3) (b). The experimental profile is indicated by (+), then calculated by (−) and the difference plot between the observed and calculated intensities is shown in each case. All the samples showed similar behavior. In these figures, an acceptable adjustment for the differences between the observed and calculated profile intensities was registered. In the insert of Fig. 3(a) and (b) an amplification of the region between 28◦ and 32◦ is presented. Here, crystallographic planes $(\bar{1}11)_m$ and $(111)_m$ confirm the presence of the ZrO_2 (1.5 mol% Y_2O_3) monoclinic phase, whereas plane $(1\ 1\ 0)_t$ indicates the presence of ZrO_2 (1.5 mol% Y_2O_3) tetragonal phase.

As observed in Fig. 3, almost flat differences were obtained between observed and calculated profile intensities. Adjustment degree for fitting patterns was from 5 to 9 (Rwp) [33].

The results of Rietveld refinements are given in Table 1. Crystallographic data, relative phase abundance and micro-strain data are given for each sample. It is evident from Table 1 that for the as-received samples series A and B that the content (wt%) of ZrO_2 (1.5 mol% Y_2O_3) solid solution is different as expected. The phase content of cubic (c-ZrO_2) and monoclinic (m-ZrO_2) polycrystals of powders (SA) is 3.6% and 2.9%,

respectively, whereas wt% for the sample (SB)was 6.7% and 6.1%. Coherent domain size or crystal size of α-Al_2O_3 crystal is close to 200 nm and does not change for the different compositions, whereas for m-ZrO_2 and c-ZrO_2 polycrystals, domain size was around 50nm and remains invariable for different compositions too. These smaller crystal sizes of ZrO_2 in Al_2O_3 matrix benefit the sintering process, by the specific surface resulting on a dividing force increase for the diffusion process [34]. No remarkable differences of unit-cell (a, b, c) parameters were found between powder samples (SA) and (SB).

However, it is evident from Table 1 that after HIP sintering at 1575 ◦C and 1600 ◦C the c value for α-Al_2O_3 crystals decreases slightly when the ZrO_2 (1.5 mol% Y_2O_3) solid solution increases from 5 wt% to 13 wt%, this smaller change in the cell can induce t-ZrO_2 micro-strain due to α-Al_2O_3 crystal relaxation through grain boundary [35]. The cell parameter a, for α-Al_2O_3 crystals remains unchanged after HIP sintering. Similar behavior was observed in other works, but in ZrO_2 crystals Y_2O_3-free [36]. The m-ZrO_2 crystals in both series SA and SB after HIP sintering process increase cell parameters. These volume expansions have been attributed to the tetragonal to monoclinic (t→m) ZrO_2 phase transformation on cooling [37]. Tetragonal polycrystals after HIP sintering at 1575 ◦C and 1600 ◦C show that the cell parameter “c” of both samples decreases slightly when the t-ZrO_2 phase increases to 11.5 wt%. A similar change is observed for cell parameter “a” of t-ZrO_2 polycrystals. The phase content of t-ZrO_2 increases from 5.5 wt% to 6.35 wt% (SA) when the temperature increased from 1575 ◦C to 1600 ◦C and α-Al_2O_3 content is around 93.4 wt%.

Table 1
Crystal structure data obtained after the Rietveld refinement of the Al_2O_3–ZrO_2 (1.5 mol% Y_2O_3) starting powders and ceramics HIP sintered at different temperatures.

	Powders		Sintering at 1575 °C (HIP)		Sintering at 1600 °C (HIP)	
	SA	SB	SA	SB	SA	SB
Lattice *a*, *b*, *c* (Å)						
r-Al_2O_3	4.7582(1), 12.9871(1)	4.7579(2), 12.9872(1)	4.7579(1), 12.9923(1)	4.7578(1), 12.9908(1)	4.7581(1), 12.9924(1)	4.7578(1), 12.9906(1)
m-ZrO_2	5.2909(1), 5.2075(3), 5.1454(1)	5.2912(1), 5.2069(2), 5.1461(1)	5.3228(3), 5.2133(7), 5.1459(1)	5.3226(4), 5.2133(8), 5.1461(3)	5.3229(3), 5.2133(1), 5.1451(7)	5.3227(4), 5.2134(8), 5.1463(3)
c-ZrO_2	5.1183(2)	5.1181(5)	–	–	–	–
t-ZrO_2	–	–	3.6043(1), 5.1954(2)	3.6036(1), 5.1931(2)	3.6043(1), 5.1953(2)	3.6038(2), 5.1928(2)
Domain size (nm)						
r-Al_2O_3	200(1)	205(1)	>1000	>1000	>1000	>1000
m-ZrO_2	51(3)	50(2)	106(3)	107(2)	101(4)	103(2)
c-ZrO_2	55(7)	54(2)	–	–	–	–
t-ZrO_2	–	–	281(4)	221(2)	289(4)	175(2)
Phase (wt%)						
r-Al_2O_3	93.5(2)	87.2(1)	93.4(1)	87.1(1)	93.4(1)	87.3(1)
m-ZrO_2	2.9(1)	6.1(1)	1.1(2)	1.4(1)	<0.5	1.2(1)
c-ZrO_2	3.6(1)	6.7(1)	–	–	–	–
t-ZrO_2	–	–	5.5(2)	11.5(1)	6.3(2)	11.5(1)
Strain (10^{-3})						
t-ZrO_2	–	–	0.59(1)	0.81(2)	0.79(1)	1.23(1)

m, monoclinic structure; t, tetragonal structure; c, cubic structure; r, rhombohedral structure.
The number between parentheses represents the error of the last number.

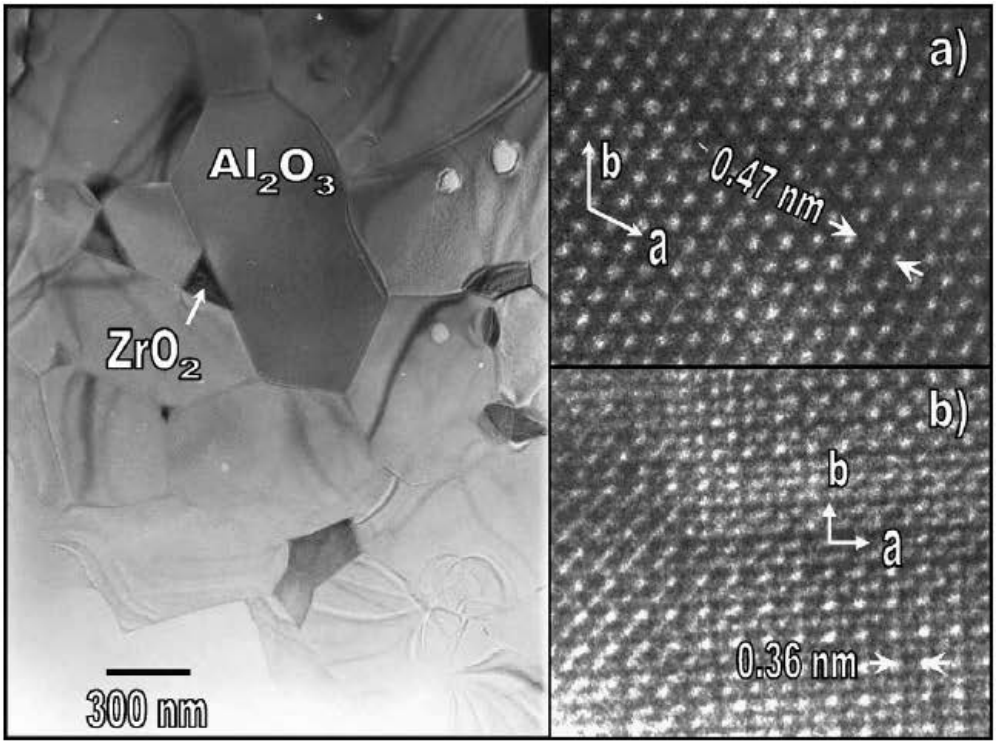

Fig. 4. Transmission electron micrograph of the Al_2O_3–13% ZrO_2 (1.5 mol% Y_2O_3) composite after HIP sintering at 1600 °C. (a) HREM image of a α-Al_2O_3 grain. (b) HREM image of a t-ZrO_2 grain.

However, when α-Al_2O_3 content decreases to around 87.1 wt% the t-ZrO_2 amount does not change with temperature (SB). The m-ZrO_2 crystal residue found in both series SA and SB varies from <0.5 wt% to 1.4wt%.

The coherent domain size after HIP sintering of α-Al_2O_3 crystals is >1000nm and around 100 nm for the m-ZrO_2 crystals (two magnitude orders from the powders). However, for tetragonal crystals it increases from 175 nm to 289nm and these values are consistent with WH values. Micro-strain values (10^{-3}) are shown in the sametable; as expectedfromWHresults, the micro-strain increases when the HIP sintering temperature and the t-ZrO_2 phase increase too. Micro-strain varies from 0.59 to 1.23 (10^{-3}); in this case, the sample with 11.5 wt% of t-ZrO_2 crystals (SB) and HIP sintering

at 1600 ◦C showed a micro-strain level slightly smaller than earlier reports with other concentrations [38].

The results of the Rietveld and Williamson–Hall methods indicated that when the amount of ZrO_2 (1.5 mol% Y_2O_3) solid solution increases from 6.5% to 12.8%, bending strength increases from 700 MPa to 1GPa. These results can be explained by amount of tetragonal phase in Al_2O_3–ZrO_2 (1.5 mol% Y_2O_3) ceramics and the presence of compressive micro-strain.

Microstructure and interface study: In order to elucidate the modifications observed in the Williamson–Hall (WH) and X-ray diffraction measurements, a morphological analysis according to TEM images was performed. For comparison effects, the “as-received” starting Al_2O_3–ZrO_2 (1.5 mol% Y_2O_3) powders were observed by means of TEM which showed irregular shape agglomeration of α-Al_2O_3 particles from 100 nm to 500nm can also be seen surrounded by minute ZrO_2 particles <100 nm.

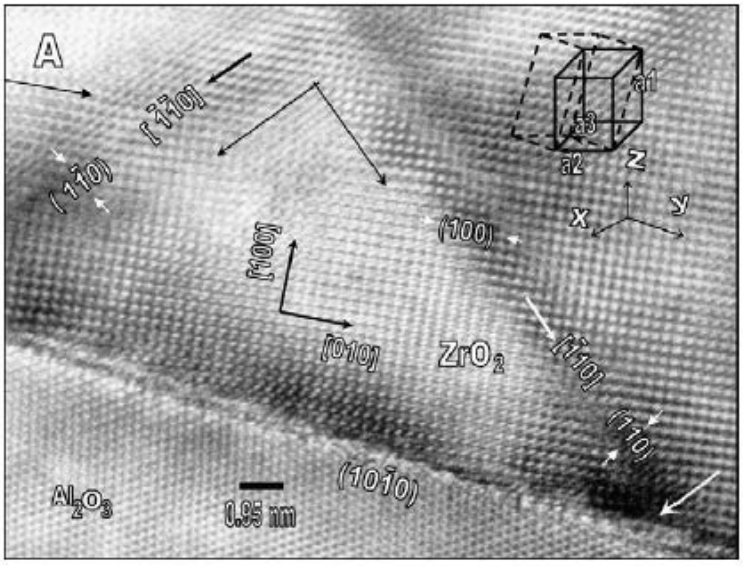

Fig. 5. HREM image of an interface between α-Al_2O_3 and t-ZrO_2 with heavily twinned structure. The observation was obtained on the $[0\,0\,0\,1]Al_2O_3 \| [0\,0\,1]ZrO_2$ zone axis.

Fig. 4 shows an example of transmission electron micrograph of as-sintered (SB) ceramic. The dark and bright grains are ZrO_2 and α-Al_2O_3 grains, respectively. In all samples sintered at 1575 ◦C and 1600 ◦C, ZrO_2 grains are located at grain boundary α-Al_2O_3 corners [39]. The alumina grain size for all sintered samples ranged from 0.5μm to 1μm. Grain sizes of ZrO_2 (1.5 mol% Y_2O_3) were smaller than those of α-Al_2O_3 (in the range 100–300 nm). Alumina grains are nearly to equiaxed form, no pores and dislocations were observed as demonstrated in Fig. 4(a) insert, and there are planes with absence of dislocations. However, ZrO_2 grains show some elongated grains due to grain coalescence and to grain growth of alumina [40]. The elongated grains show contrast lines which indicate a flow of strains and presence of dislocations, as observed in the HREM image of Fig. 4(b) insert. It is attributed mainly to strain accumulation from slip of dislocations to twining.

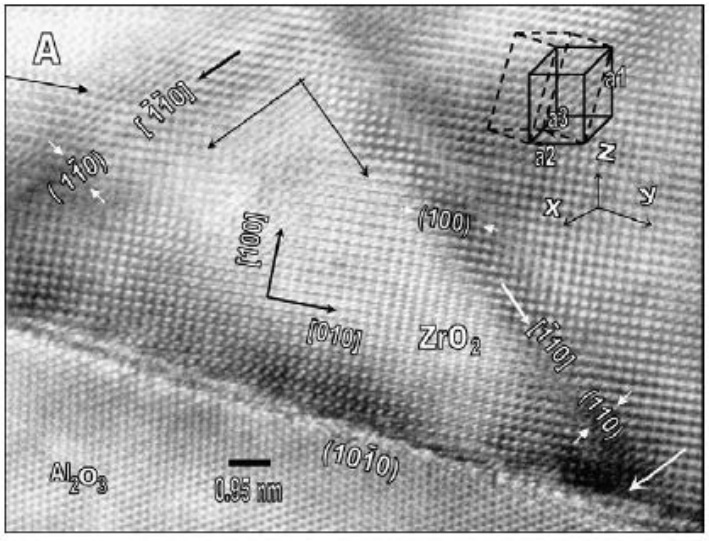

Fig. 5. HREM image of an interface between α-Al_2O_3 and t-ZrO_2 with heavily twinned structure. The observation was obtained on the $[0\,0\,0\,1]Al_2O_3 \| [0\,0\,1]ZrO_2$ zone axis.

The TEM study reveals the presence of twining in tetragonal crystals for all HIP sintering samples (generally when the orientation 0 0 ∂||00∂ is fulfilled). There is an example (SB, 1600 ◦C) in Fig. 5. This twining on the elementary cell with basis vectors a_1, a_2 and a_3 corresponds to vectors in the $[\bar{1}01)$, $[0\bar{1}0]$ and [1 0 1] crystallographic directions, respectively. The tetragonal unit cell is delineated by thick lines in Fig. 5 insert and twining shear is along $-a_1$ direction on the $a_1 \times a_2$ crystallographic plane. This can be explained by the tetragonal distortion between the family of planes {001} and {101} which are adjusted by plane shear displacements (1 1 0) and $(1\ \bar{1}\ 0)$ along $[\bar{1}\ 1\ 0]$ and $[\bar{1}\ \bar{1}\ 0]$ crystallographic directions, respectively. These planes are arrested by the $(1\ 0\ \bar{1}\ 0)$ alumina plane. These observations are consistent with the results obtained by the WH and Rietveld methods.

Fig. 6 shows a typical HREM image taken with the incident beam parallel to the $[0\ 0\ 0\ 1]Al_2O_3||[0\ 0\ 1]ZrO_2$ zone axis, together with the convergent beam electron diffraction (CBED) pattern. The interface between a twinned ZrO_2 elongated grain and an Al_2O_3 grain is shown. The boundary presents a small-angle with semi-coherent interface, in which the (1 0 0) ZrO_2 and the $(1\ 0\ \bar{1}\ 0)$ Al_2O_3 planes make an angle of about 2◦. There are no lattice deformations along the boundary.

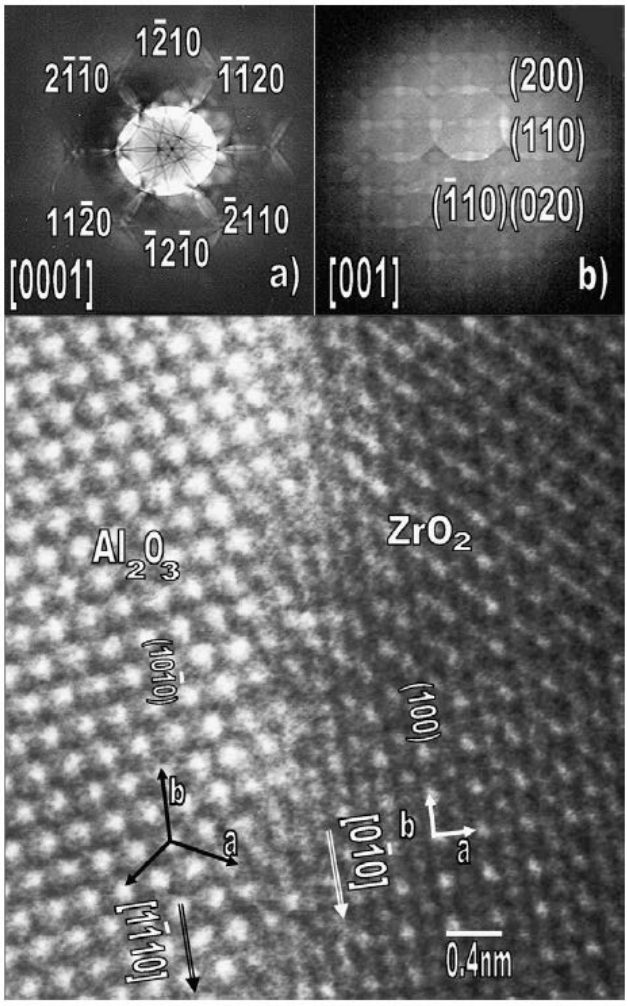

Fig. 6. HREM image of a semi-coherent α-Al_2O_3/t-ZrO_2 interface along of the $[0\,0\,0\,1]Al_2O_3||[0\,0\,1]ZrO_2$ zone axis. CBED of the (a) α-Al_2O_3 and (b) t-ZrO_2 confirm the hexagonal and tetragonal symmetry, respectively.

Conclusions

Nanometric powders and sintered ceramics Al_2O_3–ZrO_2 (1.5 mol% Y_2O_3) with 95–5 wt% and 87–13wt% concentrations have been evaluated. The relationship between microstructure and bending strength depends directly of the amount of tetragonal phase, micro-strain amount and strain orientation.

Crystallographic study indicated that the maximum bending strength it is due to accumulation of compressive micro-strain. These results can be attributed to displasive

tetragonal to monoclinic phase transformation on cooling, t-ZrO_2 grains coalescence and to α-Al_2O_3 grain growth, which causes elongated tetragonal crystals.

The results of the Rietveld and Williamson–Hall methods indicated t-ZrO_2 lattice distortion in the plane family {101} and {001}, which is presented along [1 1 0] and [0 0 1] crystallographic direction, respectively. Strong lattice distortion was obtained when the amount of tetragonal phase increased to 11.5% and it is compressive micro-strain value was around $\varepsilon = 1.2\ (10^{-3})$.

The HREM interface study conducted along [0001] Al_2O_3||[0 0 1]ZrO_2 zone axis revealed a flow of strains and presence of dislocations, which cause, micro-strain and lattice distortion accumulated close to grain boundary. It is attributed mainly to strain accumulation from dislocation slip to twining.

Acknowledgements

The authors wish to acknowledge to Tri-Osaka and Dr. Sebastián Diaz de la Torre, who supplied the materials for this study. Also,we would like to thank D. Lardizábal from Centro de Investigación en Materials Avanzados S.C. (CIMAV) and L. Rendon, R. Hernandez, P. Mexía, and C. Flores from the HRTEM Laboratory at the Instituto de Física, UNAM, México.

References

[1] S. Novak, M. Kalin, P. Lukas, G. Anne, J. Vleugels, O. Van Der Biest, J. Eur. Ceram. Soc. 27 (2007) 151.

[2] R.K. Sadangi, V. Shukla, B.H. Kear, Int. J. Refract. Metals Hard Mater. 23 (2005) 363.

[3] A.H. De Aza, J. Chevalier, G. Fantozzi, J. Am. Ceram. Soc 86 (2003) 115.

[4] D. Gutknecht, J. Chevalier, V. Garnier, G. Fantozzi, J. Eur. Ceram. Soc 27 (2007) 1547.

[5] R.H.J. Hannink, R.C. Garvie, J. Mater. Sci 17 (1982) 2637.

[6] F.Wakai, T. Nagano, T. Iga, J. Am. Ceram. Soc 80 (1) (1997) 232.

[7] R.C. Garvie, R.H. Hannink, R.T. Pascoe, Nature (London) 258 (1975) 703.

[8] D. Sarkar, S. Adak, M.C. Chu, S.J. Cho, N.K. Mitra, Ceram. Int 33 (2007) 255.

[9] K. Morita, K. Hiraga, B.-N. Kim, Acta Mater 55 (2007) 4517.

[10] D. Jiang, D.M. Hulbert, J.D. Kuntz, Mater. Sci. Eng. A 463 (2007) 89.

[11] H.S. Kim, M.Y. Seo, I.J. Kim, Am. Inst. Phys. Conf. Proc 973 (2008) 931.

[12] G.V. Srinivasan, J. Jue, S. Kuo, A.V. Virkar, J. Am. Ceram. Soc 72 (11) (1989) 2098.

[13] H. Hume, Y. Nishikawa, S. Inamura, H. Miyamoto, Rev. High Pressure Sci. Tech-355 nol 7 (1998) 1087.

[14] H.P. Klug, L.E. Alexander (Eds.), X ray Diffraction Procedure for Polycrystalline and Amorphous Materials, John Wiley & Sons, New York, 1974, pp. 682–685.

[15] B.D. Cullity (Ed.), Elements of X-ray Diffraction, M. Cohen, Addison-Wesley, Reading, MA, 1967, pp. 96–103.

[16] F.F. Bertaut, C.R. Acad. Sci. Paris 228 (187–189) (1949) 492.

[17] G.K. Williamson,W.H. Hall, Acta Metall. 1 (1953) 22.

[18] J. Rodriguez-Carvajal, Wfp2k Rietveld Program, version, Laboratorie Leon Brillouin (CEA-CNRS), 2007.

[19] National Institute of Standards and Technology, Standard Reference Material 674a, Department of Commerce, United States of America, 1989.

[20] JCPDS-International Centre for Diffraction Data, Copyright ©JCPDS-ICDD 2006, card 01-083-208.

[21] JCPDS-International Centre for Diffraction Data, Copyright ©JCPDS-ICDD 2006, card 01-070-4426.

[22] JCPDS-International Centre for Diffraction Data, Copyright ©JCPDS-ICDD 2006, card 01-077-2112.

[23] JCPDS-International Centre for Diffraction Data, Copyright ©JCPDS-ICDD 2006, card 01-072-1669.

[24] Inorganic Crystal Structure Database ICSD version 2007-2 (atomic positions).

[25] F. Sanchez-Bajo, F.L. Cumbrera, F. Guibertau, Mater. Lett. 15 (1992) 39.

[26] R. Iain, Gibson, T.S. John, Irvine J. Am. Ceram. Soc. 84 (3) (2001) 615.

[27] M. Yashima, T. Hirose, M. Kakihana, J. Am. Ceram. Soc. 80 (1) (1997) 171.

[28] F.Wakai, T. Pagano, T. Iga, J. Am. Ceram. Soc. 80 (9) (1997) 2361.

[29] N.S. Ramgir, Y.K. Hwang, I.S. Mulla, J.-S. Chang, Solid State Sci. 8 (2006) 359.

[30] J. Kishino, A. Nishiyama, J. Mater. Sci. 31 (1996) 4991.

[31] R.H.J. Hannink, P.M. Kelly, B.C. Muddle, J. Am. Ceram. Soc. 83 (3) (2000) 461.

[32] International Tables for Crystallography, 1996.

[33] A.K. Deb, P. Chatterjee, S.P. Sen Gupta, J. Appl. Crystallogr. 39 (2006) 601.

[34] J.K.M.F. Daguano, C. Santos, R.C. Souza, R.M. Palestra, Int. J. Refract. Metals Hard

Mater. 25 (2007) 374.

[35] E. Merlani, C. Schmid, V. Sergo, J. Am. Ceram. Soc. 84 (3) (2001) 2962.

[36] A.K. Deb, P. Chattrjee, S.P. Sen Gupta, Mater. Sci. Eng. A 459 (2007) 124.

[37] X.-J. Jin, Curr. Opin. Solid State Mater. Sci. 9 (2005) 313.

[38] R.C. Garvie, J. Phys. Chem. 82 (1978) 218.

[39] B.T. Lee, K. Hiraga, D. Shindo, J. Mater. Sci. 29 (1994) 959.

[40] Y. Matsomoto, K. Hirota, O. Yamaguchi, J. Kishino, J. Am. Ceram. Soc. 76 (10) (1994) 2677.